Int. J. Electrochem. Sci., 10 **(2015)** 2194 - 2205

International Journal of
ELECTROCHEMICAL
SCIENCE
www.electrochemsci.org

Effect of Adipic Acid on DEIS Characteristics during the Aluminium Anodizing Process in Sulfuric Acid Bath

Lei Hua, Jianhua Liu[*]*, Songmei Li, Mei Yu*

School of Materials Science and Engineering, Beihang University, Beijing 100191, China
[*]E-mail: liujh@buaa.edu.cn

Received: 8 December 2014 / *Accepted:* 30 December 2014 / *Published:* 19 January 2015

The formation process of anodic film on aluminium was investigated in the bath containing adipic acid and sulfuric acid (ASA bath) by using dynamic electrochemical impedance spectroscopy (DEIS). An interface reaction and ionic migration mechanism of anodic oxidation process in the ASA bath was established to interpreting the DEIS data. The impedance was decrease with the addition of adipic acid added in the anodizing bath, because of the adsorption of adipic anions on the surface of oxide film. An electrical equivalent circuit (EEC) model was established to analyse the relationship of the EEC model elements with the applied potential. The results indicated that the addition of adipic acid into the anodizing bath was beneficial to the grown of oxide film on aluminium, like faster in grown rate and thicker in thickness.

Keywords: Aluminum; Adipic-sulfuric acid anodizing; DEIS; Interface reaction

1. INTRODUCTION

The anticorrosive properties of aluminum and aluminum-based alloys are strongly increased by the anodizing process [1]. Traditional anodizing approach such as chromic acid anodizing (CAA) with thin (less than 5-6 μm) anodic films, but provide superior corrosion resistance than those produced by other anodizing processes like sulfuric acid anodizing (SAA) and phosphoric acid anodizing (PAA)[2]. However, the use of hexavalent chromium is becoming restrictive due to its characteristic as a human carcinogen and substantial contribution to environmental pollution. These disadvantages of CAA process have motivated research into development of alternative anodizing processes.

Wong and Cadwell Stancin [3,4] made efforts regarding the new anodizing processes. They invented the boric and sulfuric acid anodizing (BSA) process. The performance of the anodic films produced by BSA process such as corrosion resistance, paint adhesion, bonding strength, and effect on fatigue life are similar to the films produced by CAA process [5-7]. Therefore, BSA process has been

proposed as the preferred substitute for CAA process. Shih et al. [8] demonstrated that the microhardness and thickness of anodic films were increased when boric acid was added in the sulfuric acid as a modifier. Du et al. [5] found that the diameter of the pore layer became smaller when the alloys were anodized in the bath mixed with boric acid and sulfuric acid. In Europe, a tartaric-sulfuric acid anodizing (TSA) process has been selected to replace CAA [9-11]. Iglesias-Rubianes et al. [12] demonstrated that the addition of tartaric acid to sulfuric acid bath improved the corrosion resistance of the anodic films. Role of tartaric acid on the anodizing was suggested by Curioni et al. [9]. Partial tartaric acid were remain in the pores after anodizing, and leading to the enhanced corrosion resistance of the anodic films

Recently, adipic-sulfuric acid anodizing (ASA), an environmentally-compliant electrolyte that generates porous anodic oxide layers, has been proposed as the substitute for CAA [13,14]. The contribution of adipic acid in improving the corrosion resistance of aluminum alloys after anodizing in sulfuric acid was recognized [15]. Besides, the ASA process had little effect on fatigue life of aluminum alloys, which was similar to the CAA process [16]. However, the studies were focused on optimization of the anodizing parameters to improve corrosion resistance and to reduce the effect on fatigue life of aluminum alloys. At the present time, there is no published information about the role of adipic acid in the ASA process.

Electrochemistry impedance spectroscopy (EIS) has played an important role in analyzing charge migration between the oxide films during anodizing and simulating the structure of the oxide films. [17-23]. Furthermore, dynamic electrochemical impedance spectroscopy (DEIS) is proposed to obtain more information for non-stationary process [24,25]. This method can acquire a series impedance measurements during linear voltage sweeps, and obtaining potential dependent spectroscopy. Consequently, the aim of this work is to investigate the influence of adipic acid on charge migration and the surface charge state of the oxide films during alumiuium anodizing by means of DEIS.

2. EXPERIMENTAL

Anodizing was undertaken on superpure (φ11.3 mm × 2 mm, 99.999 % purity) aluminum specimens in 50 g/L sulfuric acid and a mixed bath (10 g/L adipic acid and 50 g/L sulfuric acid) at room temperature with a classical three-electrode cell. The aluminum specimens with an exposed area of 1 cm^2 acted as a working electrode. A saturate calomel electrode (SCE) was employed as reference and a platinum foil with 2 cm^2 surface area was used as counter electrode.

The DEIS measurements were realized under potentiodynamic conditions using a Princeton Applied Research Multichannel Potentiostats apparatus (Model VersaSTAT MC, AMETEK, Inc., United States). Each impedance spectrum was measured under a series of specific anodizing potential from open circuit potential (OCP) to 10 V. Amplitude of the sinusoidal signal superimposed on the DC anodizing potential was 10 mV, with the frequency varied between 100 kHz to 1 Hz. The impedance data was fitted using the Zsimpwin software.

The Raman spectrum was measured on a confocal micro-Raman spectrometer (Model Laboratory RAM HR800, HORIBA Jobin Yvon, France) through a 50× (NA = 0.5) microscope objective. An Ar-Kr laser, emitting at a wavelength of 514.5 nm, was used as the source of excitation.

3. RESULT AND DISCUSSION

Figure 1 shows Raman spectra for pure aluminum samples immersed in the adipic-sulfuric acid solution for 3h and for analytically pure adipic acid powder. The Raman spectrum for analytically pure adipic acid powder display the characteristics Raman peaks at about 301 cm^{-1}, 433 cm^{-1}, 1665 cm^{-1}, 1707 cm^{-1}, 1768 cm^{-1} and 2920 cm^{-1}, while the pure aluminum display the Raman peaks at about 433 cm^{-1}, 1665 cm^{-1}, 1707 cm^{-1}, and 1768 cm^{-1}. As is known, there is no response peak for pure metal on Raman spectrum. Consequently, the Raman peaks of the pure aluminum should all correspond to the characteristics Raman peaks of adipic acid. Therefore, adipic acid should be adsorbed on the surface of pure aluminum after immersion in the adipic-sulfuric acid solution.

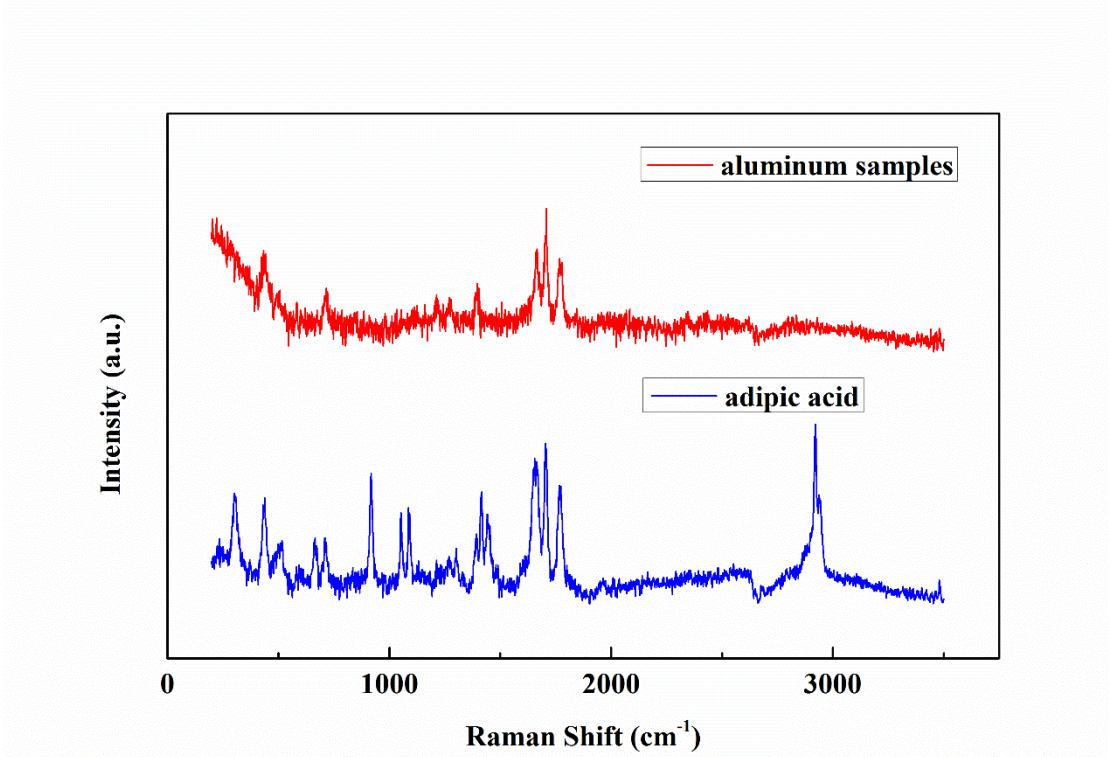

Figure 1. Raman spectra for the pure aluminum after immersion in the adipic-sulfuric acid solution for 3 h and the analytically pure adipic acid powder

Potentiodynamic conditions were applied to anodize the pure aluminum samples. As shown in Figure 2, linear anodic polarization of aluminum was performed in the bath containing 50g/L sulfuric acid with and without addition of 10 g/L adipic acid. From the commencement of anodizing, at an OCP of −0.5 V vs. SCE, the current increase rapidly until 0 V vs. SCE. Subsequently, the current reaches a plateau until 2 V vs. SCE, related to initial nonuniform film growth and thickening of the

barrier layer [26]. A transition region in which the current density increase rapidly with applied potential is observed after the plateau. The increase in current is associated with the initial growth of a porous film morphology. Finally, a mild increase in the current with the applied potential is observed above 3.5 V vs. SCE. This mild increase region is associated with the generation of the common porous morphology [10,26]. A similar overall behavior is also observed after the addition of 10 g/L adipic acid into the previous solution. In the barrier layer growth region, a little difference in the current density between SA and ASA indicates that the addition of adipic acid in bath has less effect on the growth of barrier layer. Therefore, the thickness of barrier layer is controlled solely by applied potential. The maximum thickness attainable of barrier layer is restricted to a voltage below the oxide breakdown voltage value [27]. Here, the two oxide breakdown voltage values are similar at about 2 V vs. SCE. In other words, the thickness of SA barrier layer and ASA barrier layer are similar. However, an approximately 20% decrease in the current density in transition region and mild increase region is observed. The decrease in current indicates the addition of adipic acid in sulfuric acid has an effect on the development and growth of porous anodic film.

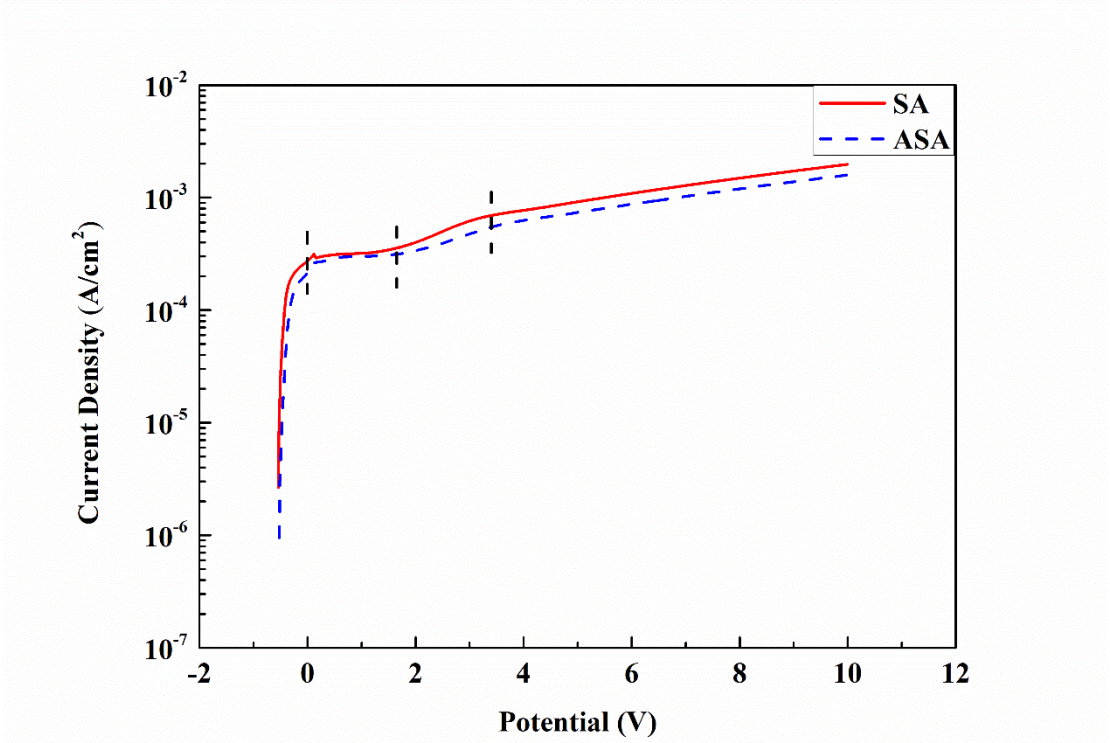

Figure 2. *I-V* behavior for the pure aluminum samples in the bath containing 50 g/L sulfuric acid with and without the addition of 10 g/L adipic acid

Figure 3 presents a series of impedance spectra in the form of Nyquist plots which are obtained under linear potential condition in different oxidation bathes. These Nyquist plots are composed of one high frequency (HF) capacitive loop, followed by a low frequency (LF) inductive loop. The phenomenon about the origin of the HF capacitive loop is attributed to charge transport process

through the aluminum oxide film [28]. While LF inductive loop is related with the relaxation of absorbed intermediates [22,29].

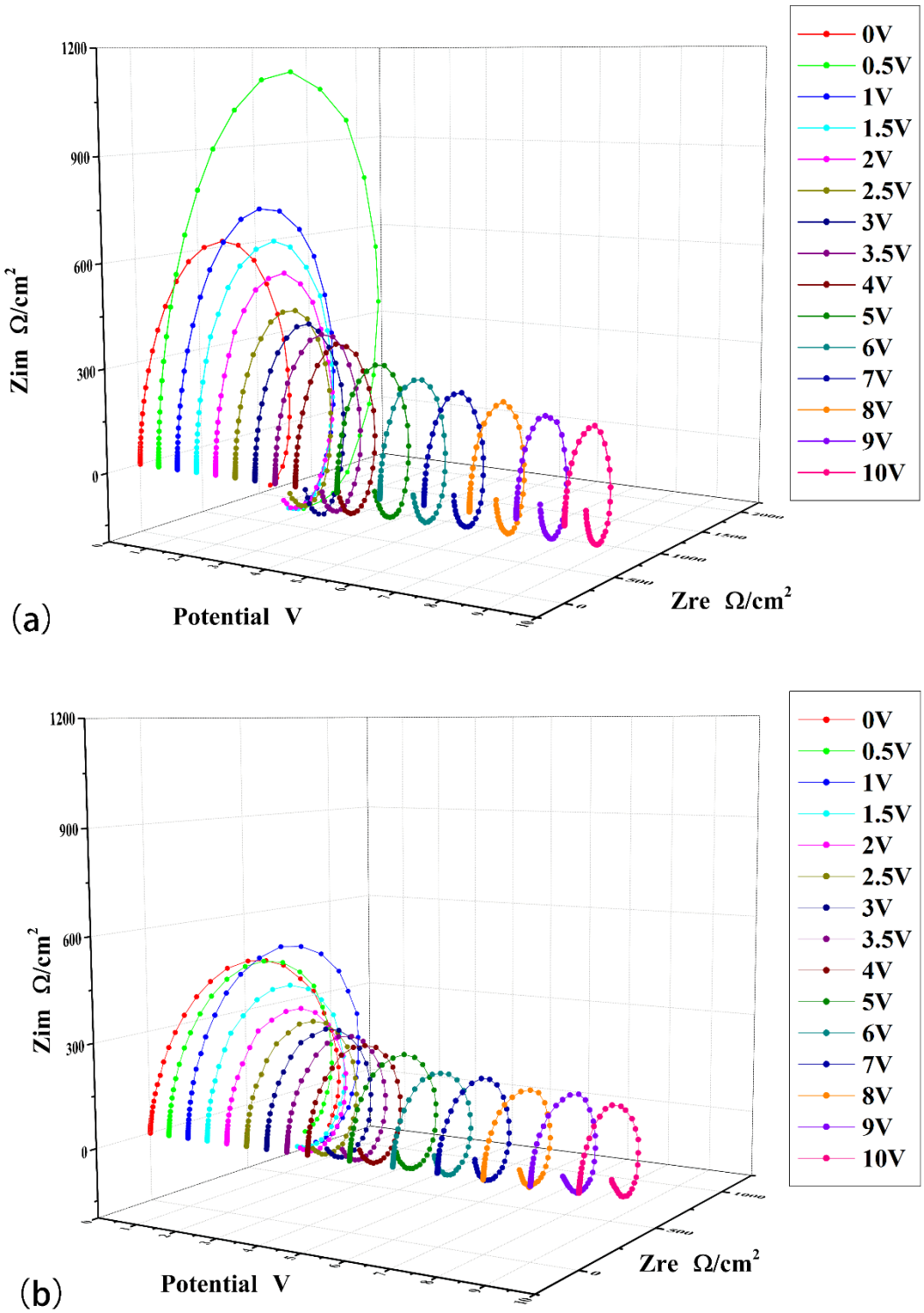

Figure 3. DEIS impedance spectra as a function of anodizing potential in different oxidation bathes: (a) sulfuric acid and (b) adipic-sulfuric acid.

Bessone et al. [20] suggested that defect chemistry should be used for interpreting impedance data of anodic film on aluminum. Both electrochemical reactions at the interfaces and ionic migration through the oxide can be incorporated into a model for anodic film growth. According to point defects model [30,31], the chemical reaction mechanism of anodic oxidation anodized in sulfuric acid can be expressed as follows:

At the metal/oxide interface (M/O):

$$Al + V_{Al}^{3'} \xrightarrow{k1} Al_{Al} + 3e^- \quad (1)$$

$$Al \xrightarrow{k2} Al_{Al} + \frac{3}{2}V_O^{''} + 3e^- \quad (2)$$

At the oxide/solution (O/S) interface:

$$Al_{Al} \xrightarrow{k3} Al^{3+} + V_{Al}^{3'} \quad (3)$$

$$H_2O \underset{k-4;k4}{\longleftrightarrow} O_{ad}^{2-} + 2H^+ \quad (4)$$

$$V_O^{''} + O_{ad}^{2-} \xrightarrow{k5} O_O \quad (5)$$

The oxide film dissolve chemical reaction:

$$[Al_{Al} + \frac{3}{2}O_O] + 3H^+ \xrightarrow{k6} Al^{3+} + \frac{3}{2}H_2O \quad (6)$$

The entity contained within the squared brackets represents the oxide lattice. Reactions (1), (3) and (5) are lattice conservative reactions which means the formed or filled of vacancies. However, reaction (2) and (6) are not lattice conservative. They will relate to the oxide growth and dissolve.

The oxygen ion vacancies are produced at the metal/oxide interface (equation (2)), but consumed at the oxide/solution interface (equation (5)). As a result, oxygen ion vacancies diffuse from the metal/oxide to the oxide/solution interface. Likewise, aluminum ion vacancies are produced at the oxide/solution interface (equation (3)), but consumed at the metal/oxide interface (equation (1)). Consequently, the aluminum ion vacancies diffuse from the oxide-solution to the metal/oxide interface. The transport of oxygen ion vacancies results in oxide growth at the metal/oxide interface (equation (2)). Similarly, (equations (1) and (3)), the transport of aluminum ion vacancies across the oxide results only in dissolution of aluminum ions at the oxide/solution interface. The fact is that only the transport of oxygen anions contributes to the film growth conflicts with the transport number of oxygen ions in an anodized layer on aluminum.

From the above reactions, the impedance can be expressed as:

$$Z = Z_{MO} + Z_f + Z_{OS} \quad (7)$$

It should be noted that this approach is only valid for quasi-equilibrium at the interfaces. The interfacial reactions are thus hardly anodic polarized. However, only the oxygen anions transport across the metal/oxide interface. The Z_{MO} can be considered to be a resistor, and be neglected further due to the fast migration rate of oxygen anions at the metal/oxide interface [21]. Therefore, the impedance can be expressed as:

$$Z = Z_f + Z_{OS} \quad (8)$$

This expression of the impedance relates to the results in figure 3 which contains two time constants.

According to de Wit [21],

$$Y_f = \frac{1}{R_f} + C_f \omega j \quad (9)$$

$$Y_{OS} = F[3k_3 b_3(1-\theta_{ao}-\theta_{aa}) + \frac{4}{3}k_5 b_5 C_O \theta_{ao}\beta]\alpha + F(3k_3 - \frac{4}{3}k_5 C_O \beta) \times \frac{k_5 b_5 C_O \theta_{ao}\beta}{\beta\omega j + k_4 + k_{-4}\beta C_H^2 + k_5 C_O \beta}\alpha + C_{OS}\omega j \quad (10)$$

where θ_{ao} is the fraction of the surface covered by adsorbed oxygen ions, θ_{aa} is the fraction of the surface covered by adsorbed anions from the electrolyte solution. C_O is the concentration of oxygen at the O/S interface. C_H is concentration of hydrogen at the O/S interface. β is the maximum number of sites per unit surface area where can be occupied by the adsorbed oxygen ions. α is the fraction of the potential drop over the O/S interface. b is the Tafel slope of the correspondent reaction.

Equation (10) can be simplified as:

$$Y_{OS} = \frac{1}{R_{OS}} + \frac{A}{B + D\omega j} + C_{OS}\omega j \quad (11)$$

where

$$\frac{1}{R_{OS}} = [3k_3 b_3(1-\theta_{ao}-\theta_{aa}) + \frac{4}{3}k_5 b_5 C_O \theta_{ao}\beta]\alpha \quad (12)$$

$$A = (3k_3 - \frac{4}{3}k_5 C_O \beta) k_5 b_5 C_O \theta_{ao}\beta\alpha \quad (13)$$

$$B = k_4 + k_{-4}\beta C_H^2 + k_5 C_O \beta \quad (14)$$

$$D = \beta \quad (15)$$

According to equation (8):

$$Z = \frac{1}{Y_f} + \frac{1}{Y_{OS}} \quad (16)$$

Then substitute equation (9) and equation (10) into equation (16), the impedance of the samples anodized in sulfuric acid can be expressed as:

$$Z = \frac{1}{\frac{1}{R_f} + C_f\omega j} + \frac{1}{\frac{1}{R_{OS}} + \frac{A}{B + D\omega j} + C_{OS}\omega j} \quad (17)$$

When the adipic acid were added into anodizing bath, the adipic acid will be ionized. The ionization balance reactions are shown in equation (18) and equation (19):

$$HOOC(CH_2)_4COOH \xleftrightarrow{k7} HOOC(CH_2)_4COO^-_{sol} + H^- \quad (18)$$

$$HOOC(CH_2)_4COO^-_{sol} \xleftrightarrow{k8} OOC(CH_2)_4COO^{2-}_{sol} + H^- \quad (19)$$

where k_7=3.7×10^{-5}, Pk_{7a}=4.43, k_8=3.9×10^{-6}, Pk_{8a}=5.41. However, the first order ionization reaction is the main reaction due to the strongly acidic anodizing bath.

Under the action of electric field force, the adipic acid anions migrate towards the surface of oxide, then adsorb on it (according to figure 2). The adsorption process is shown in equation (20).

$$HOOC(CH_2)_4COO^-_{sol} \xleftrightarrow{k9} HOOC(CH_2)_4COO^-_{ad} \quad (20)$$

As shown in Figure 4(a), the bulky adipic acid anions occupy the points where are adsorbed originally by small oxygen ions and sulfate ions. Therefore, both θ_{ao} and θ_{aa} have become smaller in equation (10). Correspondingly, the admittance Y_{OS} has become larger. In other words, the impedance

Z_{OS} has become smaller. The total impedance of the aluminum specimens anodized in ASA bath has become smaller, which is identical to the measured results in Figure 3. The decrease in θ_{ao} will result in the decrease of the reaction rate in oxide growth (equation (2) and equation (5)). Consequently, the current density of anodizing will be decreased, as shown in Figure 2.

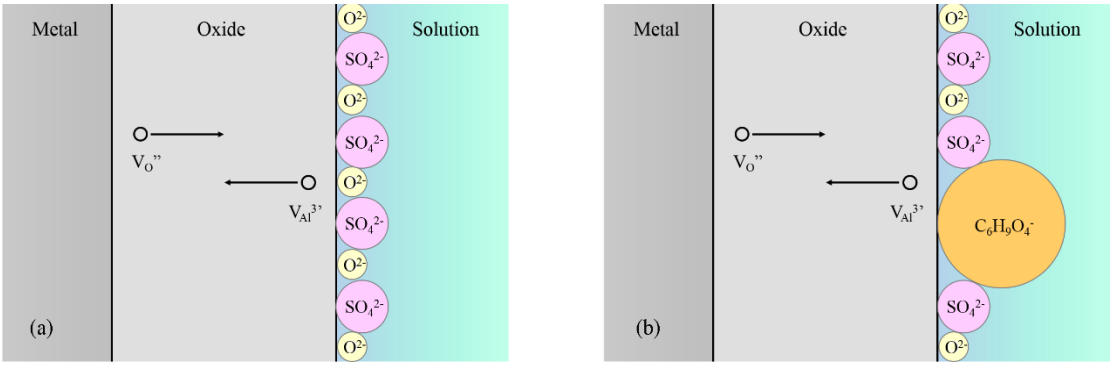

Figure 4. Ionic migration mechanism of anodic process in sulfuric acid bath (a) and adipic-sulfuric acid bath (b)

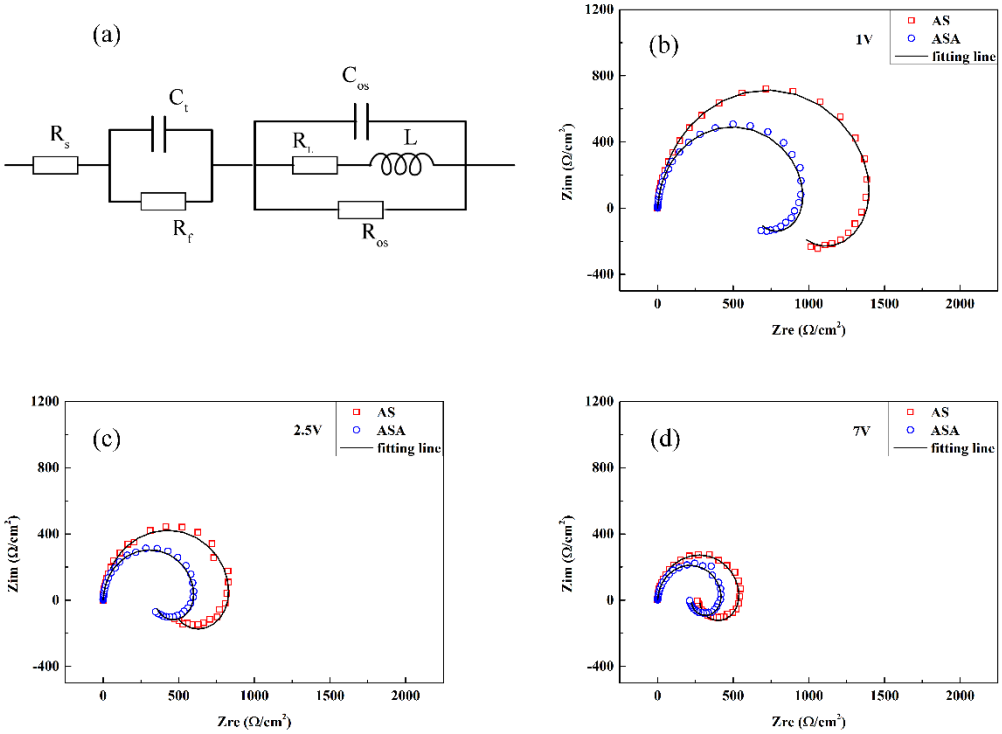

Figure 5. The fitting model (a) and the fitting results of the impedance: (b) 1 V, (c) 2.5 V and (d) 7 V

The oxide film also dissolves chemically in adipic-sulfuric acid bath. Besides reactions equation (6), equation (21) will react at the oxide/solution interface [15]:

$$[Al_{Al} + \frac{3}{2}O_O] + 3HOOC(CH_2)_4COO^-_{ad} + 3H^+ \xrightarrow{k10} Al(OOC(CH_2)_4COOH)_{3_{ad}} + \frac{3}{2}H_2O \qquad (21)$$

The production $Al(OOC(CH)_2)_4COOH$ is bulky and insoluble, absorbing on the surface of oxide as shown in figure 4(b). Therefore, the reaction rate of equation (6) slows down due to the absorbing production. The results will help the oxide grow thicker at the metal-oxide interface in ASA bath.

Two time constants could be determined from Figure 3. According to equation (9), electrical equivalent circuit (EEC) were employed to fit the EIS data, as shown in figure 5(a). The EEC is described as R(CR)(CR(LR)) by using circuit description code (CDC). The Nyquist plots at 1V, 2.5V and 7V, which are the representative potential in the barrier layer growth region, porous layer development region and porous layer growth region respectively, are selected to fit the model, as shown in Figure 5(b), Figure 5(c) and Figure 5(d). The fit results show little difference from the test results. The EEC is an appropriate model for analyzing the impedance results in more detail.

The relationship of the circuit elements with the applied potential is shown in Figure 6. Capacitance C_f is attribute to the aluminum oxide film behaving as an insulator with a dielectric constant varying between 7.5 and 12. As shown in Figure 6(a), both the C_f of oxide film anodized in SA bath (indicated by solid line) and in ASA bath (indicated by dash line) are nearly linear decrease in the barrier layer growth region. The result indicates that the thickness of barrier layer shows a linear increase with the potential increasing according to equation (22):

$$C = \frac{\varepsilon S}{4\pi k d} \qquad (22)$$

where ε is dielectric constant, S is plate area of the capacitance, d is thickness between the plates of the capacitance, k is electrostatic force constant. In the porous layer development region and porous layer growth region, both the C_f of oxide film anodized in SA bath and in ASA bath are decreased. The results indicate that the thickness of porous layer increases with the potential, but the growth rate of porous layer is slower than the growth rate of barrier layer. Figure 6(a) also shows that the C_f of oxide film anodized in ASA bath is approximately 40% lower than that in SA bath during the porous layer growth range. That is, the oxide film anodized in ASA bath is thicker than that anodized in SA bath. The insoluble $Al(OOC(CH)_2)_4COOH$ absorbing on the surface of oxide film according to equation (21) is beneficial to thickening the oxide film in ASA bath.

Resistor R_f is due to charge transport process through the aluminum oxide film, as shown in Figure 4, containing the transport of oxygen ion vacancies and aluminum ion vacancies. The transport of oxygen ion vacancies results in oxide growth at the metal/oxide interface (equation (2)). Therefore, the growth rate of oxide film can be represented by the magnitudes of R_f. In Figure 6(b), both the R_f of oxide film anodized in SA bath and in ASA bath decrease rapidly in the barrier layer growth region, and the R_f of oxide film anodized in ASA bath is approximately 65% lower than that in SA bath. The results demonstrate that the grown rate of oxide film in ASA bath is faster than that in SA bath, and the rate is faster with the increase of potential in the barrier layer growth region. Subsequently, both the R_f are decreased to a minimum value, and reach a plateau in the porous layer development region and porous layer growth region. The results demonstrate that the vacancies only transport through the barrier layer, and the grown rate increases to a maximum value. Moreover, the addition of adipic acid into the anodizing bath has reduced the transport resistor of vacancies, which increases the grown rate of porous layer.

The R_{OS} and C_{OS} in parallel represents the electric double layer at the oxide/solution surface, related to the surface reactions. Capacitance C_{OS} is differential capacitance of the electric double layer, which represents the stored energy ability when a fraction of potential generates on the surface of oxide.

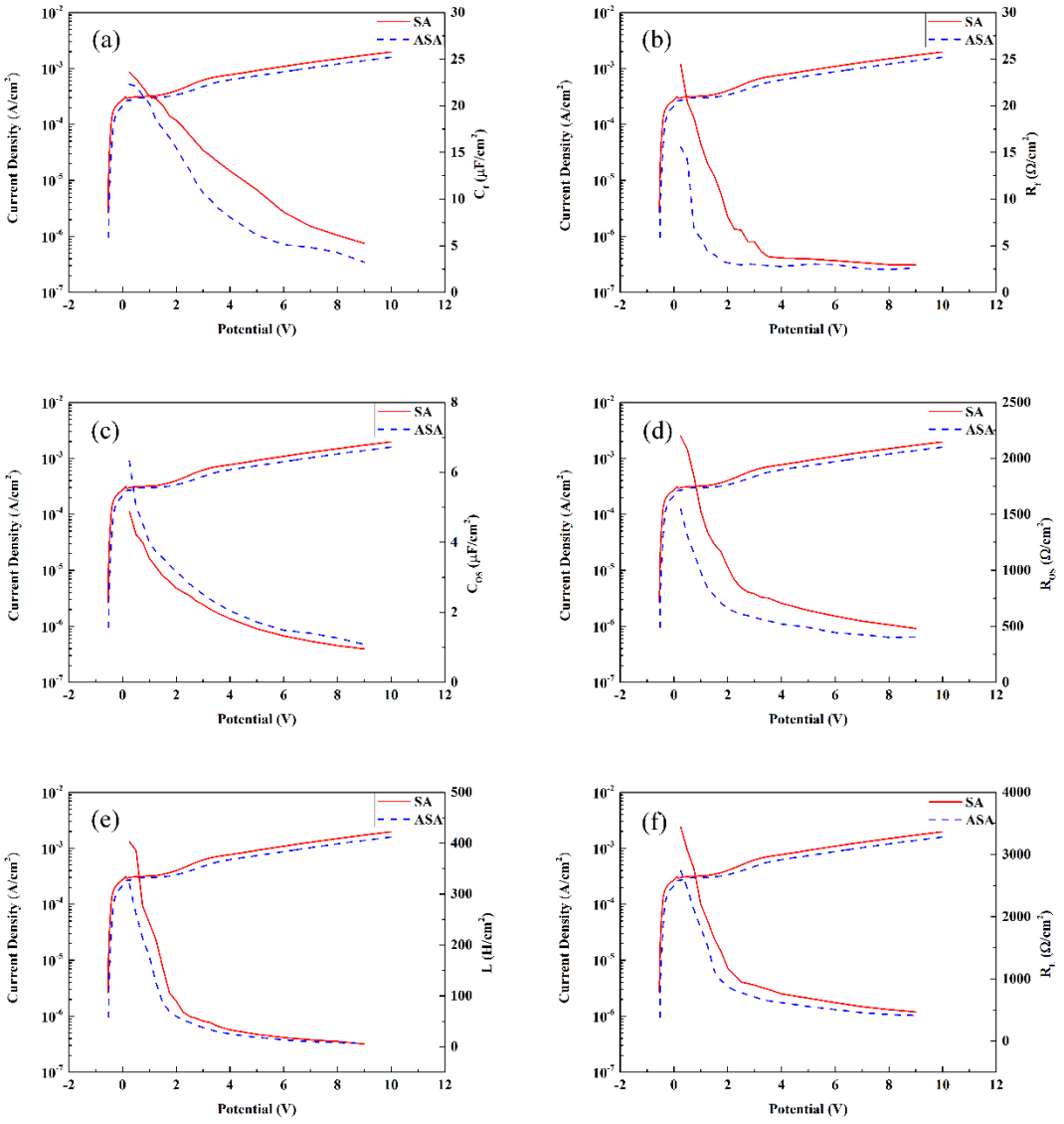

Figure 6. The relationship of the circuit elements with the applied potential: (a) C_f, (b) R_f, (c) C_{OS}, (d) R_{OS}, (e) L and (f) R_L

Resistor R_{OS} is polarization resistance of the surface reaction at the oxide/solution surface. The addition of adipic acid into the anodizing bath has increased the electric density on the surface of oxide, and has reduced the polarization resistance of the surface reactions. The results indicate that the addition of adipic acid has promoted the surface reactions due to the adsorption of adipic acid on the oxide surface.

The L and R_L in series is related with the relaxation of absorbed anions. A linear conductor mode is used to calculate the value of L in the EEC, as shown in equation (23):

$$L = l(\ln\frac{4l}{d} - 1) \times 200 \times 10^{-9} \quad (23)$$

Where l is thickness of the adsorbed layer, and d is area of the adsorbed layer. Parameter d is increase when the bulky adipic acid ion adsorb on the surface of oxide. The increase of d results in the reduction of L. Both L and R_L reach a turning point until the development of porous layer. It indicates that the anions are adsorbed mostly at the bottom of porous layer, where is equivalent to the surface of barrier layer. Moreover, the adsorbing capacity of these anions tends to be saturated until the development of porous layer.

4. CONCLUSION

We have investigated the formation process of anodic film on aluminium in the bath containing 50g/L sulfuric acid and 10g/L adipic acid. Firstly, the Raman spectrum analysis indicated that the adipic acid were adsorbed on the surface of aluminum specimens when the specimens were immersed into the ASA bath. Secondly, potentiodynamic polarization curve shown the relationship of anodizing current density and applied potential, and demonstrated the characteristic of anodizing current density in the barrier layer growth region, the porous layer development region and the porous layer growth region. Subsequently, the DEIS data were measured under potentiodynamic polarization condition. An interface reaction and ionic migration mechanism of anodic oxidation process in the ASA bath were established according to point defects model. The mechanism indicated that the decrease of impedance when the adipic acid added into the anodizing bath was due to the adsorption of adipic acid anions on the surface of oxide film. Finally, the DEIS data were fitted by an EEC model according to the interface reaction and ionic migration mechanism. The relationship of the EEC model elements with the applied potential was analyzed in contrast to the anodizing current shift in potentiodynamic polarization curve. The results indicated that the addition of adipic acid into the anodizing bath was beneficial to the grown of oxide film on aluminium, like faster in grown rate and thicker in thickness.

ACKNOWLEDGEMENTS
This research is sponsored by National Nature Science Foundations of China (NSFC, No.21371019) and Aero Science Foundation of China (ASFC, No. 2011ZE51057).

References

1. P. R. Roberge, Corrosion Engineering: Principles and Practice, McGraw–Hill: New York, 2008, pp. 603-627.
2. F. Mansfeld and M.W. Kendig, *J. Electrochem. Soc.*, 135 (1988) 828.
3. C.-M. Wong and Y. Moji, *United States Patent*, 4894127.
4. L. A. Cadwell Stancin and L. J. Douglas, *US Pantent Application Pubilication*, US 2004/0050709 A1
5. N. Du, S. Wang, Q. Zhao and Z. Shao, *Nonferro. Met. Soc. China*, 22 (2012) 1655.
6. J. Zhang, X. Zhao, Y. Zuo and J. Xiong, *Surf. Coat. Tech.*, 202 (2008) 3149.
7. L. Domingues, J.C.S. Fernandes, M. Da Cunha Belo, M.G.S. Ferreira and L. Guerra-Rosa, *Corros.*

Sci., 45 (2003) 149.
8. H. H. Shih and S. L. Tzou, *Surf. Coat. Tech.*, 124 (2000) 278.
9. S. P. A. Alenia Aeronautica, *European Patent Application*, EP 1233084 A2
10. M. Curioni, P. Skeldon, E. Koroleva, G. E. Thompson and J. Ferguson, *J. Electrochem. Soc.*, 156 (2009) C147.
11. Y. Ma, X. Zhou, G. E. Thompson, M. Curioni, T. Hashimoto, P. Skeldon, P. Thomson and M. Fowles, *J. Electrochem. Soc.*, 158 (2011) C17.
12. M. García-Rubio, P. Ocón, A. Climent-Font, R.W. Smith, M. Curioni, G.E. Thompson, P. Skeldon, A. Lavía and I. García, *Corros. Sci.*, 51 (2009) 2034.
13. J. Liu, M. Li, H. Sheng, S. Li, G. Chen and M. Yu, *Published Patent Specification*, CN101624718.
14. J. Liu, Z. Liu, M. Yu, S. Li and G. Chen, Chin. J. Nonferro. Met. 22 (2012) 2031. (in Chinese)
15. M. Yu, G. Chen, J. Liu and S. Li, *J. Beijing Univ. Aeronaut. Astronaut.*, 38(2012) 363. (in Chinese)
16. M. Yu, G. Chen, J. Liu, S. Li, Y. Li and Z, Liu, *Heat Treat. Met.*, 36(2011) 50. (in Chinese)
17. H. J. de Wit, C. Wijenberg and C. Crevecoeur, *J. Electrochem. Soc.*, 126 (1979) 779.
18. J. Bessone, C. Mayer, K. Jüttner and W. J. Lorenz, *Electrochim. Acta*, 28(1983) 171.
19. J. Hitzig, K. Jüttner, W. J. Lorenz and W. Paatsch, *Corros. Sci.*, 24(1984) 945.
20. J. B. Bessone, D. R. Salinas, C. E. Mayer, M. Ebert and W. J. Lorenz, *Electrochim. Acta*, 37(1992) 2283.
21. J. H. W. de Wit and H. J. W. Lenderink, *Electrochim. Acta*, 41(1996) 1111.
22. I. V. Aoki, M.-C. Bernard, S. I. Cordoba de Torresi, C. Deslouis, H. G. de Melo, S. Joiret and B. Tribollet, *Electrochim. Acta*, 46(2001) 1871.
23. M. Curioni, E.V. Koroleva, P. Skeldon and G.E. Thompson, *Electrochim. Acta*, 55 (2010) 7044.
24. K. Darowicki, *J. Electroanal. Chem.*, 486 (2000) 101.
25. K. Darowicki, J. Orlikowski and G. Lentka, *J. Electroanal. Chem.*, 486 (2000) 106.
26. M. Curioni, M. Saenz de Miera, P. Skeldon, G. E. Thompson and J. Ferguson, *J. Electrochem. Soc.*, 155 (2008) C387.
27. J. W. Diggle, T. C. Downie and C. W. Goulding, *Chem. Rev.*, 69 (1969) 365.
28. L. Garrigues, N. Pebere and F. Dabosi, *Electrochim. Acta*, 41 (1996) 1209.
29. S.-M. Lee and S.-I. Pyun, *J. Appl. Electrochem.*, 22 (1992) 151.
30. L. F. Lin, C. Y. Chao and D. D. Macdonald, *J. Electrochem. Soc.*, 128 (1981) 1194.
31. D. D. Macdonald, *J. Electrochem. Soc.*, 139 (1992) 3434.